Strain-modulated electron spin resonance of cubic Cr^{3+} in MgO

J. C. M. Henning and J. H. den Boef
Philips Research Laboratories, Eindhoven, The Netherlands
(Received 17 March 1978)

The novel technique of strain-modulated electron spin resonance has been used to measure the strain dependence of the g tensor of cubic Cr^{3+} centers in MgO. Writing $\delta g_i = F_{ij}\, e_j$, the coupling coefficients are found to be: $F_{11} = +0.004 \pm 0.010$, $F_{12} = -0.060 \pm 0.005$, and $F_{44} = +0.029 \pm 0.006$. As an additional result it turns out that the centers are not perfectly cubic, but are distorted by random strains. The distribution of distortions is such that the mean value of the zero-field splitting is nonvanishing. Both the mean value and the standard deviation vary from specimen to specimen and are strongly influenced by mechanical treatment. A careful examination of the spectral line positions reveals the presence of a small (cubic) $u\mu_B S\,{}^3H$ term, with $u = (+4.6 \pm 0.2) \times 10^{-5}$. The (static) g factor is $g = 1.9799 \pm 0.0001$.

I. INTRODUCTION

Chromium- (Cr^{3+}) doped MgO is an almost classical system which has been studied extensively by means of electron–spin-resonance[1-11] (ESR) and electron-nuclear-double-resonance[12] (ENDOR) techniques. Cubic[1-3,10-12] as well as tetragonal[3-6] and orthorhombic[3-9] Cr^{3+} centers have been reported. In this paper, we focus attention on the cubic centers. The chromic ion has a $3d^3$ electronic configuration. In a crystal field of cubic (octahedral) symmetry the ground state is an orbitally nondegenerate ${}^4A_2$ (${}^4F$) state with spin $S = \frac{3}{2}$. Since zero-field splittings are absent at perfectly cubic sites, the allowed ESR transitions $+\frac{3}{2} \rightarrow +\frac{1}{2}$, $+\frac{1}{2} \rightarrow -\frac{1}{2}$ and $-\frac{1}{2} \rightarrow -\frac{3}{2}$ coincide and a single ESR line results without resolved fine structure. Hyperfine interactions with neighboring ^{25}Mg nuclides have been resolved, both by means of a high-resolution ESR experiment[10] and by a double-resonance (ENDOR) technique.[12] The hyperfine splittings are small, however, and fall inside the linewidth (0.5 – 1.5 Oe) of a conventional low-resolution ESR experiment. A four-line hyperfine pattern due to the isotope ^{53}Cr ($I = \frac{3}{2}$), with a separation of about 16 Oe between successive components, is also observed.[13]

Useful information about the mechanisms leading to the energy-level splittings of Cr^{3+} in a crystalline environment can be obtained from ESR experiments under uniaxial stress. From the magnitude and the direction of the applied stress the displacements of the ligand atoms, surrounding Cr^{3+}, can be derived provided that the local-elastic-stiffness constants are known. The resulting shifts of the spectral parameters, such as g-factor and zero-field splittings, then give an indication of the change in the crystalline field due to these displacements. A difficulty is that the local elastic constants in the vicinity of the impurity ion are generally unknown. As a matter of practice they are identified with the macroscopic elastic constants of the crystal. Recent calculations by Ivanenko and Malkin[14] on rare-earth-doped fluorite crystals show that the error made with this procedure is relatively small (a few percent) for uniaxial stress along a tetragonal axis, slightly larger (20%–30%) for the shear modulus, whereas the bulk modulus may change by as much as a factor of 2. Unfortunately, no such calculations have yet been made for Cr-doped MgO, so we make the *ad hoc* assumption that c_{ij}(local) $= c_{ij}$(macroscopic).

ESR spectra with application of static uniaxial stress have been reported by Watkins and Feher.[15] They find that the major effect of stress is a shift of the zero-field splitting ($\tilde{D}$). This shift may be related to the applied elastic strain field by

$$\begin{bmatrix} \delta D_{xx} \\ \delta D_{yy} \\ \delta D_{zz} \\ \delta D_{yz} \\ \delta D_{zx} \\ \delta D_{xy} \end{bmatrix} = \begin{bmatrix} G_{11} & -\frac{1}{2}G_{11} & -\frac{1}{2}G_{11} & 0 & 0 & 0 \\ -\frac{1}{2}G_{11} & G_{11} & -\frac{1}{2}G_{11} & 0 & 0 & 0 \\ -\frac{1}{2}G_{11} & -\frac{1}{2}G_{11} & G_{11} & 0 & 0 & 0 \\ 0 & 0 & 0 & G_{44} & 0 & 0 \\ 0 & 0 & 0 & 0 & G_{44} & 0 \\ 0 & 0 & 0 & 0 & 0 & G_{44} \end{bmatrix} \begin{bmatrix} e_{xx} \\ e_{yy} \\ e_{zz} \\ e_{yz} \\ e_{zx} \\ e_{xy} \end{bmatrix} \quad (1)$$

The two independent elements of the magnetoelastic $\vec{G}$ tensor are found to be $G_{11} = +0.6$ cm^{-1}, $G_{44} = +4.2$ cm^{-1}. Apparently, the resolution of the static stress method was insufficient to detect any change in the spectroscopic splitting tensor $\vec{g}$. This is not surprising since simple crystal-field theory predicts that $F_{ij} \simeq G_{ij}/\lambda \simeq 10^{-2}$ if the strain-induced g shift is written

$$\begin{bmatrix} \delta g_{xx} \\ \delta g_{yy} \\ \delta g_{zz} \\ \delta g_{yz} \\ \delta g_{zx} \\ \delta g_{xy} \end{bmatrix} = \begin{bmatrix} F_{11} & F_{12} & F_{12} & 0 & 0 & 0 \\ F_{12} & F_{11} & F_{12} & 0 & 0 & 0 \\ F_{12} & F_{12} & F_{11} & 0 & 0 & 0 \\ 0 & 0 & 0 & F_{44} & 0 & 0 \\ 0 & 0 & 0 & 0 & F_{44} & 0 \\ 0 & 0 & 0 & 0 & 0 & F_{44} \end{bmatrix} \begin{bmatrix} e_{xx} \\ e_{yy} \\ e_{zz} \\ e_{yz} \\ e_{zx} \\ e_{xy} \end{bmatrix} . \tag{2}$$

λ is the spin-orbit coupling constant. In spite of the weakness of the effect, Walsh[16] was able to measure the shift of the isotropic g factor as a function of hydrostatic pressure. The measurements were done on powder samples at room temperature. He finds a g shift of $+2.5 \times 10^{-4}$ for a pressure of 10^{10} dyn/cm^2. In our notation this result may be written

$$F_{11} + 2F_{12} = -0.116 \pm 0.010 . \tag{3}$$

Much better sensitivity is expected from a dynamical experiment. With the recently developed[17] strain-modulated-electron-spin-resonance (SMESR) technique it is possible to detect shifts of the resonance lines as small as 10^{-3} times the linewidth. For $\Delta H_{1/2} \simeq 0.2$ Oe this means a g shift of about 10^{-7}. Since the strain in the sample is typically 10^{-5} in such experiments, F values of the order of 10^{-2} should be detectable. If the chromium ions occupy perfectly cubic sites, the effect of strain-induced $\vec{D}$ shifts cancels, since the (coinciding) transitions $+\frac{3}{2} \rightarrow +\frac{1}{2}$ and $-\frac{1}{2} \rightarrow -\frac{3}{2}$ tend to shift in opposite directions, giving rise to ac signals of opposite phase.

The objective of the experiments described in this paper is to determine the complete F tensor of Cr^{3+} at "cubic" sites in MgO, in order to provide additional experimental material for comparison with theory. Apart from these straightforward measurements, several novel features of the MgO: Cr^{3+} system are revealed. First of all, it is found that in our crystals the "cubic" Cr sites are not perfectly cubic. The distribution of distortions is such that the mean value of the zero-field splitting is nonvanishing. However, this mean value is not a material constant, but differs from sample to sample. Second, a careful examination of the spectra shows the presence of a very small $u\mu_B S^3 H$ term[18,19]; the coefficient u depends neither on the frequency[20] nor on the specimen, so it is a "real" crystal-field effect. The organization of the paper is as follows. In Sec. II A an improved version of the strain modulator is described. The equations necessary to determine the strain in the sample are also given. The experimental procedure of determining the F tensor elements is described in Sec. II B. Section III finally gives the results, together with a short discussion.

II. EXPERIMENTAL TECHNIQUE

A. SMESR apparatus

The SMESR spectrometer is essentially an X-band ($\nu \simeq 10$ GHz) homodyne mixer[21] electron-spin-resonance spectrometer, equipped with both magnetic-field and strain-modulation facilities. Since the two types of modulation occur at widely different frequencies (419 Hz and 20–100 kHz, respectively) there is no difficulty in recording both the SMESR and the "normal" ESR spectrum simultaneously. As a rule, the spectrometer is tuned to the absorption mode. The electromechanical oscillator is an improved version of the one described earlier.[17] As is shown in Fig. 1, the design is fully symmetrized, in the sense that there is a mirror plane perpendicular to the long axis at the sample position. Since both ends are free, this implies that for odd modes there is always zero displacement and maximum strain at the center of the sample. Two Piezoxide (Philips PXE-5) bimorph elements are used for producing and sensing the electromechanical vibrations. The lowest vibrational modes that can be excited with this setup are given in Table I. It is seen that a distinction between the nearby $\frac{1}{2}\lambda$ longitudinal and $n = 5$ flexural modes can be easily made by reversing the electrical connections A and B. The strain is transmitted towards the sample by a rod of fused quartz. Both the $\frac{1}{2}\lambda$ and the $\frac{3}{2}\lambda$ longitudinal extensional modes are employed in the present investigation. Figure 2 shows the way in which

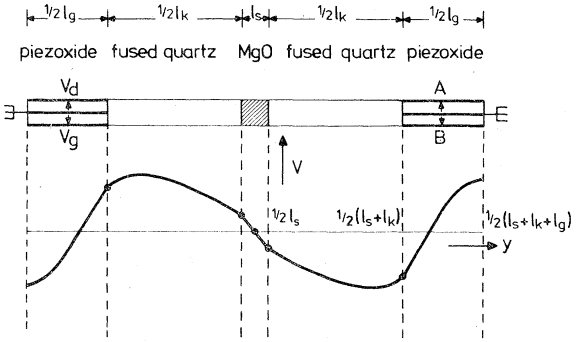

FIG. 1. Symmetrical longitudinal strain modulator. Strain is excited in two Piezoxide (Philips PXE-5) driver bars (voltage V_d) and detected in two sensor bars (V_g); A and B may be either V_d or V_g (see Table I). The polarization is indicated by arrows. Lower trace: displacement waveform for a $\frac{3}{2}\lambda$ mode. Note that the strain ($e_{yy}=dv/dy$) is discontinuous at the interfaces Piezoxide-quartz and quartz-sample.

the transducer is mounted to a specially designed TE_{102} microwave cavity. Due to the symmetrical construction the sample is always at an antinode of the radio frequency $\vec{H}_1$ field. The static magnetic field $\vec{H}$ can be rotated in the X-Z plane, perpendicular to the long axis of the transducer (Y). The transducer is kept in place by means of two Teflon slabs.

The driving voltage V_d is supplied by a voltage-tuned oscillator, the frequency of which is kept identical with the appropriate eigenfrequency of the transducer by means of a feedback loop.[22] A second loop, making use of the amplitude of V_g, controls the strain amplitude. In order to improve the accuracy of the strain measurement the sensor electrodes are connected to a probe circuitry depicted in Fig. 3. The strain in the sensor bar generates a current I_s which would produce a voltage drop V_k over the parasitic capacitance C_0 (C_0 comprises the capacity of the sensor bar, its wirings and the input capacity of the measuring instrument). This voltage drop is compensated ($V_k=0$) by a feedback system. The compensating current (I_{reg}) produces a voltage V_{gI} over a calibrated load capacitance C_L. In this way, the influence of the parasitic capacity C_0 is eliminated. The relationship between the measured voltage V_{gI} and the strain amplitude $\hat{e}_g$ in the sensor bar is easily derived from the piezoelectric equations. Consider a piezoelectric element with dimensions $t_1 \times t_2 \times t_3$ (see Fig. 4). Let the strain in the Y direction be given by

$$(e_{yy})_g = \hat{e}_g \sin(2\pi y/\lambda_g). \tag{4}$$

In the "current mode" we essentially measure the charge on the electrodes (Q),

$$Q = Y_{11} d_{31} t_1 t_2 \hat{e}_g \frac{1}{l_2 - l_1} \int_{l_1}^{l_2} \sin\left(\frac{2\pi y}{\lambda_g}\right) dy, \tag{5}$$

where d_{31} is the transverse piezoelectric charge constant and Y_{11} is Young's modulus. Introducing the "ideal transformer ratio" $N = t_2 d_{31} Y_{11}$ and re-

TABLE I. Lowest eigenmodes and frequencies of the fully symmetrized transducer of Fig. 1. Dimensions: $l_g = 25$ mm, $l_k = 34$ mm, $l_s = 3$ mm. Cross section 2×2 mm^2.

A	B	f (kHz)	Mode
V_d	V_g	2.0	$n = 1$ flexure
		11.7	$n = 3$ flexure
		27.7	$\frac{1}{2}\lambda$ long
		29.5	$n = 5$ flexure
		105	$\frac{3}{2}\lambda$ long
V_g	V_d	6.59	$n = 2$ flexure
		19	$n = 4$ flexure
		27.7	$\frac{1}{2}\lambda$ long
		40	$n = 6$ flexure
		105	$\frac{3}{2}\lambda$ long

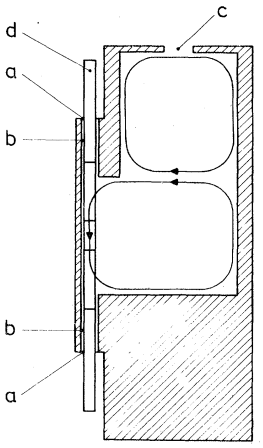

FIG. 2. TE_{102} microwave cavity with strain modulator. *a*, Teflon slabs; *b*, microwave choke; *c*, coupling iris to waveguide; *d*, transducer. The rf magnetic field lines are indicated.

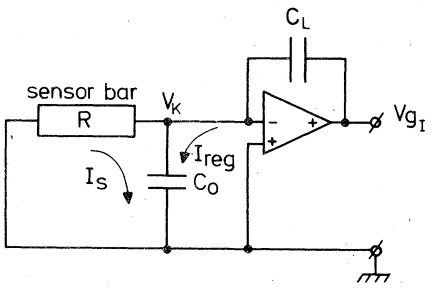

FIG. 3. Electronic probe circuit connected to sensor bar.

membering that $Q = C_L V_{gI}$, we finally arrive at

$$\hat{e}_g = \frac{2\pi\sqrt{2}C_L(V_{gI})_{\rm rms}}{N\lambda_g[\cos(2\pi y/\lambda_g)]I_1^2}. \tag{6}$$

It should be noted that in our actual setup, two sensor bars are used in parallel, so the right-hand side of Eq. (6) has to be divided by 2. Since low-temperature data of Piezoxide are not available from the manufacturer, we calibrated our transducer at $T = 77$ K and find $N = 1.21 \times 10^{-2}$ N/m (±10%) and for the velocity of sound: $v_g = 3324$ m/sec in Piezoxide and $v_k = 5500$ m/sec in fused quartz.

The final problem is to relate the strain in the sensor bar ($\hat{e}_g$) to the strain in the sample ($\hat{e}_s$). The solution is straightforward if we impose the conditions of continuity of displacement and of stress at each of the interfaces Piezoxide-quartz and quartz-sample, respectively. This leads to a set of two homogeneous linear equations, which are soluble if the resonance condition

$$\frac{\lambda_g}{Y_g}\cot\left(\frac{\pi l_g}{\lambda_g}\right) = \frac{\lambda_s \sin(\pi l_s/\lambda_s)\cos(\pi l_k/\lambda_k) + (Y_s/Y_k)\lambda_k \cos(\pi l_s/\lambda_s)\sin(\pi l_k/\lambda_k)}{-Y_k(\lambda_s/\lambda_k)\sin(\pi l_s/\lambda_s)\sin(\pi l_k/\lambda_k) + Y_s\cos(\pi l_s/\lambda_s)\cos(\pi l_k/\lambda_k)} \tag{7}$$

is satisfied. The required relationship between $\hat{e}_s$ and $\hat{e}_g$ then reads

$$\frac{\hat{e}_s}{\hat{e}_g} = \frac{\lambda_g \cos(\pi l_g/\lambda_g)}{\lambda_s \sin(\pi l_s/\lambda_s)\cos(\pi l_k/\lambda_k) + \lambda_k(Y_s/Y_k)\cos(\pi l_s/\lambda_s)\sin(\pi l_k/\lambda_k)}. \tag{8}$$

This relationship was checked experimentally by replacing the sample by an auxiliary Piezoxide sensor. The agreement between calculated and measured strain is better than 2%.

B. Determination of the F tensor

The ESR spectrum of Cr^{3+} ($3d^3$) in MgO can be described by the spin Hamiltonian

$$\mathcal{H} = \mu_B \vec{H}\cdot\vec{\vec{g}}\cdot\vec{S} + \vec{S}\cdot\vec{\vec{D}}\cdot\vec{S} + u\mu_B\{S_\xi^3 H_\xi + S_\eta^3 H_\eta + S_\zeta^3 H_\zeta - \tfrac{1}{5}(\vec{S}\cdot\vec{H})[3S(S+1)-1]\}, \tag{9}$$

where μ_B is the Bohr magneton and ξ, η, ζ refer to the cubic ⟨100⟩ axes. For sites with cubic symmetry, we expect an isotropic g tensor and $D_{ij} = 0$. The transitions $+\frac{1}{2} \rightarrow +\frac{3}{2}$ and $-\frac{1}{2} \rightarrow -\frac{3}{2}$ then coincide but, as a rule, they will not coincide with the $-\frac{1}{2} \rightarrow +\frac{1}{2}$ transition as a consequence of the $u\mu_B S^3 H$ term.

The major effect of strain modulation will be a modulation of the tensors $\vec{\vec{D}}$ and $\vec{\vec{g}}$. For small strains, the shifts of these tensors may be linearly related to the applied elastic strain, as was done in Eqs. (1) and (2). For cubic crystals, the F tensor has three independent elements: F_{11}, F_{12}, and F_{44}. A relationship, analogous to $G_{12} = -\frac{1}{2}G_{11}$ does not hold for the F tensor, since $\delta\vec{\vec{g}}$ is not traceless. This is clearly demonstrated by Walsh's hydrostatic experiments [Eq. (3)]. Three independent measurements are therefore necessary to determine the F tensor completely.

In a dynamical experiment g shifts are measured by comparing the intensities of the strain-modulated ESR signals (I_s) with those of the H-modulated signals (I_e). If the overall gains of the SMESR (G_s) and "normal" ESR (G_e) spectrometers are calibrated, an effective strain-modulation depth m_s can be defined

$$m_s = m_e(I_s/I_e)(G_e/G_s), \tag{10}$$

where m_e is the magnetic field modulation depth. This equation should be corrected for passage effects, if present.[17] The g shift (δg) follows from

$$\delta g = g m_s/H. \tag{11}$$

In the experiments, described in Sec. III, the stress (T_{yy}) is applied either along the [010], the [111], or the [110] direction. The magnetic field vector $\vec{H}$ is rotated in the X-Z plane, perpendicular to the stress axis (Y). The relevant expressions of the effective F value for each of these cases will now be derived.

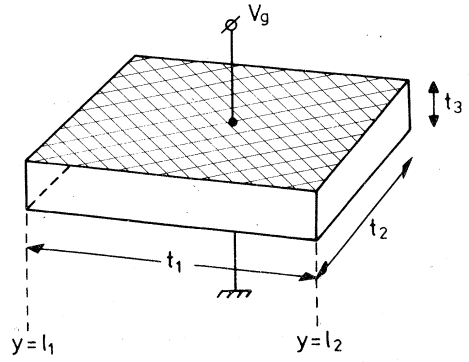

FIG. 4. Geometry of Piezoxide bar.

1. Stress $T_{yy} \parallel [010]$

The cubic axes (ξ, η, ζ) can be identified with the laboratory axes (X, Y, Z). It follows that $e_{xx} = e_{zz} = s_{12}T_{yy}$, $e_{yy} = s_{11}T_{yy}$. Using Eq. (2) we then find

$$\delta g_{xx} = \delta g_{zz} = (F_{11}s_{12} + F_{12}s_{11} + F_{12}s_{12})(e_{yy}/s_{11}) , \quad (12)$$
$$\delta g_{xz} = 0 .$$

The g shifts are isotropic for $\vec{H}$ rotating in the X-Z plane.

2. Stress T_{yy} ∥[111]

The laboratory frame is chosen so that Y coincides with the stress axis [111], $X = [1\bar{1}0]$ and $Z = [11\bar{2}]$. Referred to the cubic axes we then have $e_{\xi\xi} = e_{\eta\eta} = e_{\zeta\zeta} = \frac{1}{3}T_{yy} \times (s_{11} + 2s_{12})$, $e_{\xi\eta} = e_{\eta\zeta} = e_{\zeta\xi} = \frac{1}{3}T_{yy}s_{44}$. The corresponding g shifts are:

$$\delta g_{\xi\xi} = \delta g_{\eta\eta} = \delta g_{\zeta\zeta} = \tfrac{1}{3}(F_{11} + 2F_{12})(s_{11} + 2s_{12})T_{yy}$$
$$\delta g_{\zeta\xi} = \delta g_{\xi\eta} = \delta g_{\eta\zeta} = \tfrac{1}{3}F_{44}s_{44}T_{yy} .$$

Transforming the g tensor to the laboratory frame we arrive at

$$\delta g_{xx} = \delta g_{zz} = [(F_{11} + 2F_{12})(s_{11} + 2s_{12}) - F_{44}s_{44}] \times (s_{11} + 2s_{12} + s_{44})^{-1}e_{yy} , \quad (13)$$
$$\delta g_{xz} = 0 .$$

Again, we find an isotropic g shift for $\vec{H}$ rotating in the X-Z plane.

3. Stress T_{yy} ∥[110]

With $X = [1\bar{1}0]$, $Y = [110]$, and $Z = [001]$ the strains in the cubic coordinate system are given by: $e_{\xi\xi} = e_{\eta\eta} = \frac{1}{2}T_{yy}(s_{11} + s_{12})$, $e_{\zeta\zeta} = T_{yy}s_{12}$, $e_{\xi\eta} = \frac{1}{2}T_{yy}s_{44}$, $e_{\eta\zeta} = e_{\zeta\xi} = 0$. The nonvanishing g shifts in the cubic frame are then

$$\delta g_{\xi\xi} = \delta g_{\eta\eta} = \tfrac{1}{2}(F_{11} + F_{12})(s_{11} + s_{12})T_{yy} + F_{12}s_{12}T_{yy} ,$$
$$\delta g_{\zeta\zeta} = \tfrac{1}{2}F_{12}(s_{11} + s_{12})T_{yy} + F_{11}s_{12}T_{yy} ,$$
$$\delta g_{\xi\eta} = \tfrac{1}{2}F_{44}s_{44}T_{yy} .$$

After transformation to the laboratory frame we find

$$\delta g_{xx} = [\tfrac{1}{2}(F_{11} + F_{12})(s_{11} + s_{12}) + F_{12}s_{12} - \tfrac{1}{2}F_{44}s_{44}] \times [\tfrac{1}{2}(s_{11} + s_{12}) + \tfrac{1}{4}s_{44}]^{-1}e_{yy} ,$$
$$\delta g_{zz} = [\tfrac{1}{2}F_{12}(s_{11} + s_{12}) + F_{11}s_{12}] \times [\tfrac{1}{2}(s_{11} + s_{12}) + \tfrac{1}{4}s_{44}]^{-1}e_{yy} , \quad (14)$$
$$\delta g_{xz} = 0 .$$

Apparently, an anisotropic g shift can be expected in this case.

III. RESULTS AND DISCUSSION

The MgO samples used in this work were kindly supplied by Dr. van Wieringen. The preparation of the single crystals has been described in Ref. 2. The samples contain many iron-group impurities like Cr, Mn, V, Fe in concentrations of the order of 1–10 ppm. The exact impurity levels differ from sample to sample. Six distinct crystals were used for the measurements. They were cut in rectangular blocks with dimensions 2 × 2 × (3–10) mm, the longest edge being along the stress direction (Y).

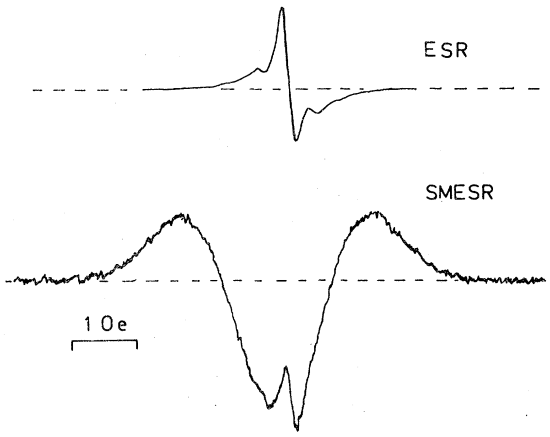

FIG. 5. ESR spectrum ($d\chi''/dH$ vs H) of cubic Cr^{3+} in MgO for $\vec{H}$ ∥ [100], $T = 77$ K, $\nu = 10$ GHz. *Upper trace*: H-modulated ESR. The shoulders are due to badly resolved shfs with Mg^{25} nuclides. *Lower trace*: first-harmonic SMESR.

Typical Cr^{3+} ESR and SMESR spectra for $\vec{H}$ ∥ [100], $\nu = 10$ GHz and $T = 77$ K are shown in Fig. 5. The ESR trace shows a single narrow line (linewidth $\Delta H_d = 170$ mOe) with partly resolved ^{25}Mg superhyperfine structure. In the SMESR spectrum the narrow line is superimposed on a broad background with a peculiar shape. Apparently, the narrow central line has to be identified with the $-\frac{1}{2} \rightarrow +\frac{1}{2}$ transition of Cr^{3+}, whereas the broad line represents the remaining $\pm\frac{1}{2} \rightarrow \pm\frac{3}{2}$ fine-structure transitions. In Sec. III A we first concentrate on the strain dependence of the $-\frac{1}{2} \rightarrow +\frac{1}{2}$ transition. In Sec. III B the peculiarities, of the broad line will be described.

A. F tensor

The F tensor is evaluated by comparing the ESR and SMESR intensities of the narrow $-\frac{1}{2} \rightarrow +\frac{1}{2}$ line. In principle, the method is straightforward; the recipe has been given in Sec. II B. A practical difficulty is, however, that the F values of Cr^{3+} are rather small so that we should be aware of possible spurious effects.

First of all, we have checked that the present setup is free of frequency and angular modulation.[23] If the transducer is not properly cemented, e.g., if there are cracks in the bonds, an inhomogeneous stress field may result, which immediately shows up in a pathological angular depen-

dence of the SMESR signal heights.

Since ESR and SMESR spectra are recorded at different modulation frequencies, improper I_s/I_e ratios may result as a consequence of rapid passage.[17,24] This can be avoided by keeping the microwave power at a low enough level ($P_0 < 5$ μW in all our measurements).

A very troublesome effect is breakaway of dislocations from their pinning points.[25-27] This leads to uncontrollable values of the local strain components. The effect is readily recognized in a SMESR experiment by observing the onset of nonlinearities both in the internal friction $(V_d - V_s)$ and in the strain-sensitivity $(I_s - V_s)$. F measurements can therefore not be made at strain levels exceeding 5×10^{-6}. Since the Cr concentration of the crystals is rather low (a few ppm) this means that we have to content ourselves with poor signal-to-noise ratios. A favorable exception to this rule is the configuration with stress along a [111] direction. In this orientation amplitude-dependent damping and irreproducibilities were not observed up to the maximum attainable strain amplitude (6×10^{-5}). This can be easily explained by realizing that the slip system in MgO consists of {110} planes with Burgers vectors along $\langle 1\bar{1}0 \rangle$. In a stress field $\vec{\mathrm{T}}$ a dislocation line experiences a force component

$$\vec{f} = \sigma \vec{b} \tag{15}$$

along the Burgers vector $\vec{b}$. Here, the resolved shear stress σ is given by[28]

$$\sigma = \vec{n} \cdot \vec{\mathrm{T}} \cdot \vec{b}/|\vec{b}|\,, \tag{16}$$

where $\vec{n}$ is the normal to the glide plane. From Eqs. (15) and (16) it is easily seen that the force on each dislocation vanishes if $\vec{\mathrm{T}}$ is either a uniaxial stress along [111] or a hydrostatic pressure. The hydrostatic-pressure experiment of Walsh[16] and our measurements with $T \parallel [111]$ are therefore considered as the most reliable data.

Measurements with stress along [110], [010], and [111] give rise to four effective F_H^T values, F_{001}^{110}, $F_{1\bar{1}0}^{110}$, F^{010}, and F^{111}, which are related to the tensor elements F_{11}, F_{12}, and F_{44} through Eqs. (12)–(14). The elastic constants of MgO at $T = 77$ K are taken from Schawlow *et al.*[29]: $s_{11} = 3.884 \times 10^{-13}$, $s_{12} = -0.867 \times 10^{-13}$, and $s_{44} = 6.671 \times 10^{-13}$, all figures in cm^2/dyn. Each measurement was repeated several times. In all cases the SMESR signal was in phase with and proportional to the applied strain, at least for small strains. The sign of the F_H^T figures was determined absolutely by going carefully through all phase shifts.

The experimental results are

$$F_{1\bar{1}0}^{110} = -0.045 \pm 0.005\,, \quad F_{001}^{110} = -0.020 \rightarrow 0.110\,,$$

$$F^{010} = -0.050 \pm 0.008, \quad F^{111} = -0.042 \pm 0.003\,.$$

The indicated error margins show that F^{111} is the most accurate measurement, F^{010} and $F_{1\bar{1}0}^{110}$ are usable although less accurate, but the results for $T \parallel [110]$ and $\vec{\mathrm{H}} \parallel [001]$ are irreproducible even if we compare subsequent measurements on the same crystal. We therefore thought it wise to omit the data of F_{001}^{110} and to combine the remaining SMESR data with Walsh's hydrostatic-pressure experiment [Eq. (3)]. In doing so, we obtain an overdetermined set of four-linear equations in three unknowns, which can be solved with the least-squares method.[30] The result is

$$F_{11} = +0.004 \pm 0.010, F_{12} = -0.060 \pm 0.005,$$

$$F_{44} = +0.029 \pm 0.006\,.$$

The value of F_{001}^{110} calculated with these parameters is -0.030 and lies within the range of experimental values.

A direct confrontation of these results with theory is impracticable since calculated F values are not available in the literature. However, it is possible to make a link between our F_{44} value and the stress-induced splitting of the ^2E state, measured by Schawlow, Piksis, and Sugano.[29] For $T \parallel [111]$ this splitting has been interpreted[31] in terms of two stress-induced trigonal field parameters $v_s = -0.77 \times 10^{-8}$ and $v_s' = +0.68 \times 10^{-8}$ cm^{-1}/dyn cm^{-2}. On the theoretical side, MacFarlane[32] has shown that the g anisotropy $(g_\parallel - g_\perp)_s$ is connected with v_s and v_s' through

$$\frac{2(g_\parallel - g_\perp)_s}{\bar{g} - g_0} = \frac{3\sqrt{2}v_s'}{10D_q + 12B} - \frac{v_s}{10D_q}\,. \tag{17}$$

Inserting $10Dq = 16\,600$ cm^{-1}, $10Dq + 12B = 24\,400$ cm^{-1}, $\bar{g} - g_0 = -0.02$, and the above-mentioned values of v_s and v_s', we arrive at $(g_\parallel - g_\perp)_s = 1.6 \times 10^{-14} = F_{44}s_{44}$ which leads to $F_{44} = +0.024$. This figure compares remarkably well with our result.

B. Further details of the spectrum

The shape of the broad line, observed in the SMESR spectrum for $\vec{\mathrm{H}} \parallel [001]$ (Fig. 5) can be understood as a superposition of two lines with equal height and opposite phase, which are shifted with respect to each other. These two lines are quite naturally attributed to the transitions $-\frac{1}{2} \rightarrow -\frac{3}{2}$ and $+\frac{1}{2} \rightarrow +\frac{3}{2}$ of Cr^{3+}, which are expected to give signals of opposite phase as a consequence of $\vec{\mathrm{D}}$ modulation (see Sec. I). The increased width of these fine-structure transitions as compared with that of the central $-\frac{1}{2} \rightarrow +\frac{1}{2}$ line points to inhomogeneous broadening. The physical mechanism of broadening may be either strain broadening

due to dislocations or point defects or broadening due to electric fields or field gradients.[33] In the vicinity of the [001] axis the splitting $\Delta_{001}/g\mu_B = H(\frac{3}{2} \rightarrow \frac{1}{2}) - H(-\frac{1}{2} \rightarrow -\frac{3}{2})$ and the linewidth were determined by means of a line-shape simulation. Both parameters appear to be specimen dependent and are strongly influenced by mechanical treatment of the crystals. This suggests that dislocations play a dominant role. Typical splittings occurring in our measurements are in the range between −2 and +3 Oe. The sign of Δ_{001} is found by comparing the phase of the broad line with that of the narrow central line. The linewidth observed for $\vec{H} \| [001]$ varies between 2 and 4 Oe.

For $\vec{H} \| [001]$ the splitting Δ_{001} induced by random strains ϵ_{ij} is given by

$$\Delta_{001} = 6G_{11}(\langle\epsilon_{zz}\rangle - \tfrac{1}{2}\langle\epsilon_{xx}\rangle - \tfrac{1}{2}\langle\epsilon_{yy}\rangle). \qquad (18)$$

A nonvanishing value of Δ_{001} is therefore not expected in a perfectly cubic crystal, where $\langle\epsilon_{xx}\rangle = \langle\epsilon_{yy}\rangle = \langle\epsilon_{zz}\rangle$. A possible way out is the assumption that the dislocation distribution is inhomogeneous. As a matter of fact, x-ray topography studies by Lang and Miuscov[34] show that the dislocations are distributed inhomogeneously and are concentrated into polygonal cell walls within individual subgrains. A trivial contribution to Δ_{001} may also arise from an inhomogeneous bias stress caused by cementing the crystal in between two quartz rods.

When $\vec{H}$ is rotated away from the [001] axis, the two fine-structure transitions shift towards each other and broaden. The angular dependence of the linewidth can therefore best be studied by recording the second harmonic SMESR signal, in which both transitions add with equal phases. Typical results are presented in Fig. 6, where the full linewidth at half-height $\Delta H_{1/2}$ of the second harmonic SMESR signal is plotted versus angle ϑ for $\vec{H}$ rotating in the (010) and (110) planes, respectively. It is to be noted that Figs. 6(a) and 6(b) refer to different crystals. The experimental results are compared with an analytical expression for the second moment derived by Feher and Weger[35,36] assuming a Gaussian distribution of internal stresses. On symmetry grounds, it can be shown that for cubic crystals the relationship should be of the form

$$\langle(g\mu_B\delta H)^2\rangle = A + B(\alpha_1^2\alpha_2^2 + \alpha_2^2\alpha_3^2 + \alpha_3^2\alpha_1^2), \qquad (19)$$

where α_1, α_2, α_3 are the direction cosines of $\vec{H}$ with respect to the cubic axes. In the model of Feher and Weger the coefficients are found to be

$$A = \tfrac{27}{2}\alpha^2\left(\frac{G_{11}}{c_{11}-c_{12}}\right)^2, \quad B = 36\mu_B^2\left(\frac{G_{44}}{c_{44}}\right)^2 - 3A. \qquad (20)$$

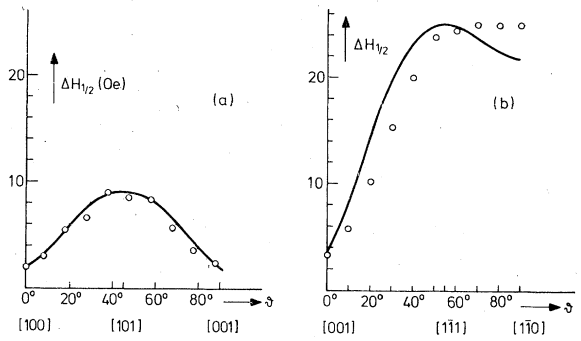

FIG. 6. (a) Angular dependence of linewidth $\Delta H_{1/2}$ of second-harmonic SMESR line for $\vec{H}$ rotating in a (010) plane. Data for one of the "best" crystals; (b) $\Delta H_{1/2}$ vs ϑ for $\vec{H}$ in a (110) plane. Data for one of the "worst" crystals.

The assumption, implicit in the derivation of Eq. (20) is that the stochastic variations of the Cartesian stress components are uncorrelated; the standard deviations of the diagonal and nondiagonal components of the random stress are denoted by α and β, respectively. Figure 6 shows that the agreement between theory and experiment is good for crystal a, but only qualitative for crystal b. The standard deviations derived for the two crystals are $\alpha_a = 1.8 \times 10^8$, $\beta_a = 1.0 \times 10^8$, and $\alpha_b = 3.1 \times 10^8$, $\beta_b = 2.4 \times 10^8$, all figures in dyn cm^{-2}. Defining with Stoneham[33] $\epsilon_{001} = 2\epsilon_{zz} - \epsilon_{xx} - \epsilon_{yy}$ and $\epsilon_{111} = \epsilon_{xy} + \epsilon_{yz} + \epsilon_{zx}$, we find for the width of the stochastic strain distributions $\sigma(\epsilon_{001}) = 2.1 \times 10^{-4}$, $\sigma(\epsilon_{111}) = 1.1 \times 10^{-4}$ (ratio of 1.9) for crystal a and $\sigma(\epsilon_{001}) = 3.6 \times 10^{-4}$, $\sigma(\epsilon_{111}) = 2.8 \times 10^{-4}$ (ratio of 1.3) for crystal b. Theoretically,[33] the ratio $\sigma(\epsilon_{001})/\sigma(\epsilon_{111})$ should be 2.3 for broadening caused by homogeneously distributed dislocations with Burgers vectors along ⟨110⟩. Apparently, this assumption holds better for crystal a than for crystal b.

A check on the assignment of the broad line to $\pm\frac{1}{2} \rightarrow \pm\frac{3}{2}$ transitions of Cr^{3+} can be made by comparing the strain sensitivity with the known[15] G_{ij} values of this ion. Unfortunately, a direct accurate determination of the G_{ij} is impracticable since the broad line does not show up in the ESR spectrum. Nevertheless, it is possible to check our assignment by observing the overmodulation threshold of the second-harmonic SMESR signal height I_{s2}.[37] Since $\omega_s T_1 > 1$ (fast passage) a plot of I_{s2} versus the strain-modulation voltage V_g exhibits a maximum when the modulation depth m_s equals the width of the spin packets. The V_g value at which a maximum occurs is then inversely proportional to the effective G value for the particular orientation of $\vec{H}$ and stress axis. The G_H^T

values, thus obtained may be compared with calculated values. In order to avoid the difficulty of determining the width of the spin packets it is convenient to compare ratios of G_H^τ values, instead of absolute values. Experimentally we find, for instance, $G_{001}^{110}/G_{001}^{001}=1$ (1), $G_{1\bar{1}0}^{110}/G_{001}^{110}=13$ (14) and $G_{1\bar{1}0}^{110}/G_{1\bar{1}0}^{111}=2$ (1.4), where the "theoretical" ratios are given in parentheses. The agreement is satisfactory and corroborates our interpretation.

A final detail of the spectra is the asymmetrical position of the $+\frac{1}{2}\rightarrow-\frac{1}{2}$ transition (H_s) with respect to the center of gravity of the broad line (H_c). This asymmetry is most clearly seen for $\vec{H}\|[100]$, when the broad line has minimum width (Fig. 5). For this orientation we find $H_s-H_c=+0.25\pm0.01$ Oe. For $\vec{H}\|[111]$ the shift is negative: $H_s-H_c=-0.17\pm0.04$ Oe. The latter measurement is less accurate as a consequence of the greater linewidth. The most natural explanation of this asymmetry is the assumption that terms of the form $u\mu_B S^3 H$ are present in the spin Hamiltonian. Terms of this kind are allowed for systems with spin $S\geq\frac{3}{2}$,[18,19] and have therefore been included in our phenomenological spin-Hamiltonian Eq. (9). Theoretically[38,39] the separation H_s-H_c is given by

$$H_s-H_c=(3uH/g)p(\alpha_1,\alpha_2,\alpha_3), \qquad (21)$$

with

$$p(\alpha_1,\alpha_2,\alpha_3)=1-5(\alpha_1^2\alpha_2^2+\alpha_2^2\alpha_3^2+\alpha_3^2\alpha_1^2).$$

Since $p([100])=1$ and $p([111])=-0.67$, we expect that the shift H_s-H_c for $\vec{H}\|[111]$ will be -0.67 times the shift at $\vec{H}\|[100]$, in agreement with the observations. The value of u was obtained from the more accurate measurement at $\vec{H}\|[100]$: $u=(+4.6\pm0.2)\times10^{-5}$. This figure may be compared with theoretical estimates by Szymczak[40] who reports u values of the order of 10^{-5} for Cr^{3+} in ruby and in emerald. It has recently been pointed out by Gehlhoff[20] that experimentally determined u values might contain a spurious contribution from local lattice distortions. Since these "spurious" u contributions vary inversely with the square of the magnetic field, they can be distinguished from the "real" crystal-field u value by doing measurements at different microwave frequencies. Measurements at frequencies between 8 and 10 GHz show that the u value is independent of the frequency and therefore must be due to a "real" crystal-field effect. After correction for the $u\mu_B S^3 H$ effect the g factor is found to be $g=1.9799\pm0.0001$.

ACKNOWLEDGMENT

The authors are indebted to R. P. van Stapele for clarifying discussions.

[1] W. Low, Phys. Rev. 105, 801 (1957).
[2] J. S. van Wieringen and J. G. Rensen, in *Paramagnetic Resonance*, edited by W. Low, (Academic, New York, 1960), Vol. I, p. 105.
[3] J. E. Wertz and P. Auzins, Phys. Rev. 106, 484 (1957); J. Phys. Chem Solids 28, 1557 (1967).
[4] S. A. Marshall, J. A. Hodges, and R. A. Serway, Phys. Rev. A 136, 1024 (1964).
[5] B. Henderson and T. P. P. Hall, Proc. Phys. Soc. 90, 511, (1967).
[6] K. P. O'Donnell, M. O. Henry, B. Henderson, and D. O'Connell, J. Phys. E 10, 3877 (1977).
[7] J. H. E. Griffith and J. W. Orton, Proc. Phys. Soc. 73, 948 (1959).
[8] A. J. B. Codling and B. Henderson, J. Phys. C 4, 1242 (1971).
[9] J. J. Davies and J. E. Wertz, J. Phys. C 8, 1235 (1975).
[10] J. C. M. Henning and J. H. den Boef, Phys. Lett. A 59, 241 (1976).
[11] J. P. Larkin, G. F. Imbusch, and F. Dravnieks, Phys. Rev. B 7, 495 (1973).
[12] P. Freund (private communication, and unpublished).
[13] G. A. Woonton and G. L. Dyer, Can. J. Phys. 45, 2265 (1967).
[14] Z. I. Ivanenko and B. Z. Malkin, Sov. Phys.-Solid State 11, 1498 (1970).
[15] G. D. Watkins and E. R. Feher, Bull. Am. Phys. Soc. 7, 29 (1962).
[16] W. M. Walsh, Phys. Rev. 122, 762 (1961).
[17] J. C. M. Henning and J. H. den Boef, Phys. Rev. B 14, 26 (1976).
[18] B. Bleaney, Proc. Phys. Soc. 73, 939 (1959).
[19] G. F. Koster and H. Statz, Phys. Rev. 113, 445 (1959); 115, 1568 (1959).
[20] W. Gehlhoff, Phys. Status Solidi B 80, 549 (1977).
[21] T. H. Wilmshurst, *Electron Spin Resonance Spectrometers* (Hilger, London, 1967), Ch. 3.
[22] J. H. den Boef and J. C. M. Henning, in *Proceedings of the Eighteenth Colloque Ampère, Nottingham, 1974* (North Holland, Amsterdam, 1975).
[23] J. H. den Boef and J. C. M. Henning, Rev. Sci. Instrum. 45, 1199 (1974).
[24] R. R. Ernst and W. A. Anderson, Rev. Sci. Instrum. 36, 1696 (1965).
[25] J. S. Koehler, in *Imperfections in Nearly Perfect Crystals*, edited by W. Shockley *et al.* (Wiley, New-York, 1952), p. 197.
[26] A. Granato and R. Lücke, J. Appl. Phys. 27, 583 (1956); 27, 789 (1956).
[27] W. H. Robinson and H. K. Birnbaum, J. Appl. Phys. 37, 3754 (1966).
[28] F. R. N. Nabarro, *Theory of Crystal Dislocations* (Clarendon, Oxford, 1967).
[29] A. L. Schawlow, A. H. Piksis, and S. Sugano, Phys. Rev. 122, 1469 (1961).
[30] E. R. Cohen and J. W. Dumond, *Encyclopedia of Physics*, edited by S. Flügge (Springer, Berlin, 1957), Vol. XXXV, p. 53—66.
[31] R. M. MacFarlane, Phys. Rev. 158, 252 (1967).
[32] R. M. MacFarlane, Phys. Rev. B 1, 989 (1970).

[33]A. M. Stoneham, Revs. Mod. Phys. 41, 82 (1969).
[34]A. R. Lang and V. F. Miuscov, Philos. Mag. 10, 263 (1964).
[35]E. Rosenvasser Feher, Phys. Rev. A 136, 145 (1964).
[36]E. R. Feher and M. Weger, Bull. Am. Phys. Soc. 7, 613 (1962).
[37]J. C. M. Henning and J. H. den Boef, Phys. Status. Solidi B 72, 369 (1975).
[38]J. C. M. Henning, H. van den Boom, and J. Dieleman, Philips Res. Rep. 21, 16 (1966).
[39]F. S. Ham, G. W. Ludwig, G. D. Watkins, and H. H. Woodbury, Phys. Rev. Lett. 5, 468 (1960).
[40]H. Szymczak, *Proceeding of the Sixteenth Colloque Ampère, Bucharest, 1970* (Publishing House of the Socialist Republic of Romania, 1971) p. 723.